Understanding the interactions between oxygen vacancies at SrTiO_{3} (001) surfaces

Houlong L. Zhuang, P. Ganesh, Valentino R. Cooper, Haixuan Xu, and P. R. C. Kent

Phys. Rev. B **90**, 064106 — Published 11 August 2014

DOI: 10.1103/PhysRevB.90.064106

Understanding the Interactions Between Oxygen Vacancies at $SrTiO_3$ (001) Surfaces

Houlong L. Zhuang,[1,*] P. Ganesh,[1,†] Valentino R. Cooper,[2] Haixuan Xu,[3] and P. R. C. Kent[4,1]

[1]*Center for Nanophase Materials Sciences, Oak Ridge National Laboratory, Bethel Valley Road, Oak Ridge, Tennessee 37831, United States*

[2]*Materials Science and Technology Division, Oak Ridge National Laboratory, Bethel Valley Road, Oak Ridge, Tennessee 37831, United States*

[3]*Department of Materials Science and Engineering, The University of Tennessee, Knoxville, Tennessee 37996, United States*

[4]*Computer Science and Mathematics Division, Oak Ridge National Laboratory, Bethel Valley Road, Oak Ridge, Tennessee 37831, United States*

We examine the role of neutral divacancies on the electronic and atomic structure at $SrTiO_3$ (001) surfaces using a density-functional theory + U approach. Our results show that the interactions between divacancies are significantly less repulsive at the SrO-terminated surface (0.05 eV) than at the TiO_2-terminated one (0.38 eV), mainly due to the increased electrostatic screening at the ionic SrO-layer compared to the covalently bonded TiO_2 layer. The interaction energies are a non-monotonic function of distance, with the fourth nearest-neighbor oxygen-oxygen divacancy showing a significantly reduced repulsion at 0K on the TiO_2-terminated surface where the defects are in the equatorial oxygen plane. This enhanced reduction in the repulsive interaction is a consequence of the much larger reduction in local symmetry relative to other divacancy arrangements arising from strong coupling with in-plane octahedral distortions. On the SrO-terminated surface, due to increased electrostatic screening, the interaction energy begins to decrease beyond the third nearest neighbor. On both surfaces, the reduced repulsion (0.05 eV and 0.38 eV) should permit oxygen vacancy ordering at finite temperatures. Finally, we discuss the emergence of a two-dimensional electron gas due to oxygen divacancies at both the TiO_2- and SrO-terminated $SrTiO_3$ (001) surfaces and contrast them with the case of a single oxygen vacancy. Neutral oxygen vacancies on the SrO-termination leads to more electron localization than on the TiO_2 surface. These results suggest an explanation for the local ordering observed in experiment, thereby highlighting the importance of ordering both for enhanced conductivity and carrier densities at oxide surfaces and at heterostructure interfaces.

I. INTRODUCTION

The discovery of a two-dimensional electron gas (2DEG) at the $SrTiO_3/LaAlO_3$ interface,[1] has motivated many investigations to understand this phenomenon. 2DEGs have also been discovered in heterointerfaces with other band insulators such as $LaGaO_3$.[2] Interfaces between STO and Mott insulators, e.g., $SrTiO_3/LaNiO_3$, also show an increase in conductivity.[3] While oxygen vacancies are not in general thermodynamically stable at oxide surfaces and interfaces,[4,5] they are metastable during and after growth. The level of metallicity is strongly dependent on the growth conditions. For example, growth under oxygen poor conditions leads to increased interfacial free-electron densities, by nearly two orders of magnitude relative to oxygen rich conditions.[6]

Surprisingly, experiments show that even bare STO surfaces can generate 2DEGs[7,8] and δ-doping can further lead to superconductivity.[9] Although the mechanism of the presence of 2DEG at STO surfaces remains unclear, oxygen vacancies have been suggested to play a central role.[7,8,10] Previous theoretical works have addressed the importance of a single oxygen vacancy in creating 2DEGs at STO surfaces.[11,12] Hybrid density functional theory (DFT) calculations suggest that a single neutral oxygen vacancy introduces a defect state $\sim$0.57 eV below the conduction band minimum.[13,14] The vacancy is thought to be a n-typed donor with a localized spin-polarized electron deep in the in-gap state and another electron delocalized in the conduction band minimum states. However, experiments also indicate the presence of ordered vacancies, both in bulk perovskite oxides and at oxide heterostructures.[15–19] Regions with ordered oxygen vacancies in $YMnO_3$ are found to be conducting,[20] implying that ordered vacancies may also be metallic. A theoretical study of oxygen vacancies in bulk $CaMnO_3$ suggests that the ordering of vacancies is favored at finite temperatures.[21] This makes it necessary to quantify the interactions between oxygen vacancies even at bare STO surfaces and understand their effects on structural- and electronic-reconstructions.

In this paper, we quantify the interactions between oxygen vacancies as a function of separation on the SrO- and TiO_2- terminated surfaces of STO in order to understand how the interactions in different divacancy arrangements couple to the underlying atomic- and electronic-structure. We observe that the interactions between divacancies are significantly less repulsive at the SrO-terminated surface (0.05 eV) than at the TiO_2-terminated surface. This is possibly due to the ionic nature of the SrO-layer. In addition, at the TiO_2-terminated surface the fourth nearest-neighbor oxygen divacancy has a significantly reduced repulsion at 0K, i.e. 0.38 eV, less than the other divacancies considered, implying that vacancies can order at STO surfaces at finite temperatures. Here, divacancies which result in signifi-

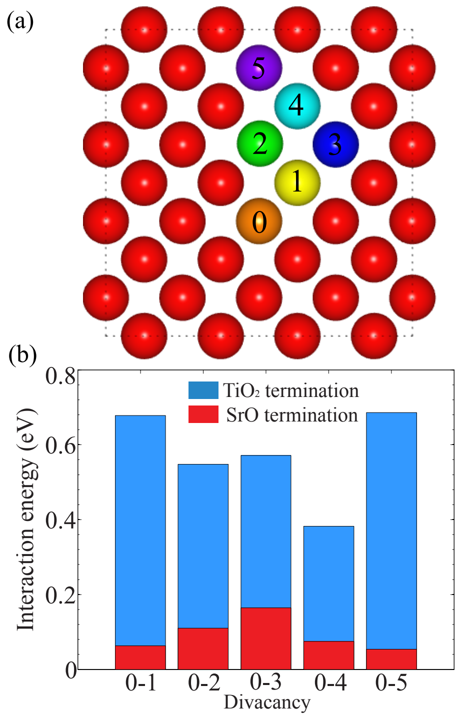

FIG. 1. (a) Oxygen sublattice at the topmost layer of STO (001) surfaces. Zero indicates the location of the first oxygen vacancy, while the other numbers denote the positions of the second vacancy in order to form a divacancy at the surface. (b) Calculated interaction energies between the vacancies forming the various divacancies at TiO_2 and SrO terminated surfaces.

cant symmetry breaking due to larger distortions of the neighboring Ti-centered octahedra lead to larger reductions in the vacancy-vacancy repulsion. This feature is most significant for vacancies ordered along the <1,3> direction. In addition, all possible divacancy arrangements lead to the emergence of 2DEGs; thus explaining the increased conductivity observed in oxide heterostructures grown under oxygen poor conditions that also show ordered vacancy arrangements.[15,16,20] The largest contribution to the 2DEG is mainly from the pristine TiO_2 layer closest to the defective layer. The SrO-layer never contributes to the metallicity due to its intrinsic ionicity. In addition, nature of electron localization is very different on the two different terminations. This implies that while the 2DEG at ABO_3 oxide heterostructure interfaces can arise from neutral oxygen vacancies, the contribution to the metallicity comes from the the closest lying BO_2 layers. While electrons tend to delocalize occupying high mobility metallic bands on the TiO_2-terminated surface, for the SrO-termination vacancies lead to strongly localized heavy bands. This might be the reason why heavy bands are seen in addition to lighter metallic bands.

II. METHODS

We perform DFT calculations using the projector augmented wave method as implemented in the plane-wave code VASP.[22–24] The Sr $4s4p5s$, Ti $3p3d4s$, and O $2s2p$ electrons are treated as valence electrons. To deal with the localized d electron states in Ti, we utilize the Dudarev method with an onsite Coulomb interaction $U = 5.0$ eV and on-site exchange interaction $J = 0.64$ eV,[25] consistent with the U and J values commonly used in other reports.[11,26] For all calculations, a cutoff energy of 500 eV for the plane wave basis set is used to converge the total energy to within 1 meV per formula unit. To model a single oxygen vacancy in bulk STO, we use a $4 \times 4 \times 4$ supercell. For the simulations of surface vacancies, we use a 4×4 supercell in the in-plane directions and nine atomic layers along the STO <001> direction. This large in-plane supercell is chosen to minimize the interactions of vacancies with their periodic images. Each surface slab consists of two symmetric surfaces with or without vacancies. As a result, the surface slabs without vacancies and with TiO_2 or SrO terminations contain 368 and 352 atoms, respectively. A vacuum spacing of 20 Å ensures that the interactions between the two symmetric surfaces are negligible. The k-point sampling uses the Monkhorst-Pack scheme[27] and employs a Γ-point-centered $8 \times 8 \times 8$ mesh for the unit cell of bulk STO and Γ-point-centered $2 \times 2 \times 1$ mesh for surface calculations. The atomic positions of the middle three layers in the surface slabs are fixed to their bulk positions, whereas all the other atomic positions are optimized until the interatomic forces are smaller than 0.03 eV/Å.

Similar to previous studies,[11,12] we consider both the TiO_2 and SrO surface terminations, which have also been experimentally observed by scanning tunneling microscopy.[28] To facilitate ensuing discussions of various divacancies at the (001) surfaces, we notice that oxygen atoms in the topmost layer of the TiO_2- or the SrO-terminated surfaces occupy the sites of a square lattice, as illustrated in Fig. 1(a). The distance between nearest-neighbor oxygen atoms in this square lattice is a_0 for the SrO-termination and $a_0/\sqrt{2}$ on the TiO_2-terminated surface, where a_0 is our relaxed bulk STO lattice parameter 3.968 Å. This is close to the experimental lattice parameter of 3.905 Å and similar to other DFT studies. We fix the first isolated oxygen vacancy at site 0, then the second isolated oxygen vacancy is located at the sites varying from 1 to 5. Consequently, each divacancy can be explicitly identified by a two-digit notation. For example, the 0-4 divacancy represents the fourth nearest neighboring oxygen vacancy with reference to the 0 reference vacancy site.

III. RESULTS

We first compute the formation energy E_f of a single oxygen vacancy in bulk STO and at its (001) surfaces with the two types of terminations. Within bulk STO, E_f is calculated as,[29]

$$E_f^{\rm bulk} = E_{\rm bulk}(1V_{\rm O}) - E_{\rm bulk}(0V_{\rm O}) + \mu_{\rm O}, \quad (1)$$

where $E_{\rm bulk}(1V_{\rm O})$ and $E_{\rm bulk}(0V_{\rm O})$ are the total energies of the $4 \times 4 \times 4$ STO supercells with and without an oxygen vacancy, respectively. $\mu_{\rm O}$ is the temperature (T) and pressure (P) dependent chemical potential of oxygen defined as:[30]

$$\mu_{\rm O} = \frac{1}{2}E_{\rm O_2} + \Delta\mu_{\rm O}(T,P) \quad (2)$$

Similarly, the surface vacancy formation energy for our symmetric surface is defined as,[31]

$$E_f^{\rm surface} = \frac{1}{2}(E_{\rm surface}(2V_{\rm O}) - E_{\rm surface}(0{\rm V}_{\rm O}) + 2\mu_{\rm O}), \quad (3)$$

where $E_{\rm surface}(2V_{\rm O})$ is the total energy of a STO surface slab containing two symmetric single vacancies. $E_{\rm surface}(0V_{\rm O})$ is the total energy of a pure STO surface.

To define the relevant range of $\mu_{\rm O}$ in Eqs. 1 and 3, we take into account both the upper and lower limits of $\mu_{\rm O}$, corresponding to O-rich and O-poor conditions, respectively.[32] The upper limit is set to half of the DFT total energy of an oxygen molecule $E_{\rm O_2}$, and all values of $\mu_{\rm O}$ are reported relative to this upper limit. The lower limit is determined as one third of the formation-energy of bulk cubic STO, i.e.

$$\mu_{\rm O} = \frac{1}{3}(E_{\rm STO} - E_{\rm Sr} - E_{\rm Ti} - \frac{3}{2}E_{\rm O_2}), \quad (4)$$

where $E_{\rm STO}$, $E_{\rm Sr}$, and $E_{\rm Ti}$ are the total energies for the bulk phases of STO, Sr, and Ti, respectively. Equation 4 yields -4.30 eV $\leq \Delta\mu_{\rm O} \leq 0$ eV.

Figure 2 shows the calculated bulk and surface vacancy formation energies as a function of $\mu_{\rm O}$. The bulk vacancy formation energy is the highest in bulk STO for the same oxygen chemical potential, indicating that an oxygen vacancy forms more readily at surfaces than in the bulk, due to the reduced coordination. Comparing the two surface vacancy formation energies, we see that oxygen is more easily removed from the TiO_2-terminated surface than from the SrO-terminated surface. This is because the SrO layer is strongly ionic leading to stronger Sr-O bonds than Ti-O bonds in the covalent TiO_2 layer. Indeed, in the same rock-salt structure, the formation energy of SrO is higher (-6.14 eV) than TiO (-5.62 eV).[33] The more covalent nature of the Ti-O bond in STO is further supported by the large Born effective charge observed for the Ti cations. Although it is more difficult to create a single oxygen vacancy on the SrO-terminated surface due to its ionicity, the same ionicity helps in screening the interactions between oxygen divacancies, as we will see shortly below.

A range of calculated values for $E_f^{\rm bulk}$ have been reported using different methods.[13,14,31,34–36] For example, Scuseria and coworkers[13] employed the hybrid DFT to

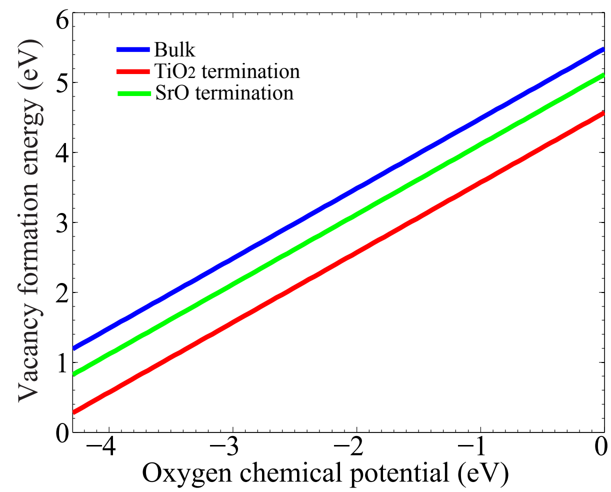

FIG. 2. Bulk and surface vacancy formation energies of $SrTiO_3$ as a function of oxygen chemical potential.

obtain a maximum $E_f^{\rm bulk} = 7.43$ eV, under oxygen rich conditions. Wang and coworkers[31] report a value 4.40 eV for the bulk using the O_2 molecule for the oxygen reference by PBE+U, with U=4.5 eV. Mitra et al.[14] report a neutral vacancy formation energy of 6 eV by hybrid DFT, referenced to the oxygen molecule. Ertekin and coworkers[36] discussed many of the uncertainties and sources of variance in these studies in their analysis of a range of neutral and charged defects. These include variations due to the use of different DFTs, supercell sizes, and any corrections applied, e.g., for the formation energy of the oxygen molecule which is not well reproduced in PBE[37] and not corrected within a DFT+U scheme.

Our calculated limits of $E_f^{\rm bulk}$, i.e. 1.19 eV $< E_f^{\rm bulk} <$ 5.48 eV are in reasonable agreement with the above literature. In contrast, few studies have provided the vacancy formation energies at STO (001) surfaces. For instance, Ref. [12] determines $E_f^{\rm surface}$ as 2.92 and 4.40 eV for TiO_2 and SrO-terminated surfaces, respectively, using PBE DFT. Both values lie within the limits of our calculated surface vacancy formation energies shown in Fig. 2.

We next calculate the interaction energy $E_{\rm int}$ between two single vacancies at the STO (001) surfaces. $E_{\rm int}$ is evaluated according to the following formula,[38]

$$E_{\rm int} = \frac{1}{2}(E_{\rm surface}(4V_{\rm O}) + E_{\rm surface}(0{\rm V}_{\rm O}) - 2E_{\rm surface}(2V_{\rm O})), \quad (5)$$

where $E_{\rm surface}(4V_{\rm O})$ is the total energy of a STO surface consisting of two equivalent divacancies on the top and the bottom of the slab. This corresponds to measuring the interactions between surface divacancies with respect to two non-interacting isolated surface vacancies on the same type of surface termination. The factor of two in Eq.5 occurs because we use symmetric surfaces for all slabs with/without vacancies. A similar equation is used to describe the interactions between two isolated oxygen

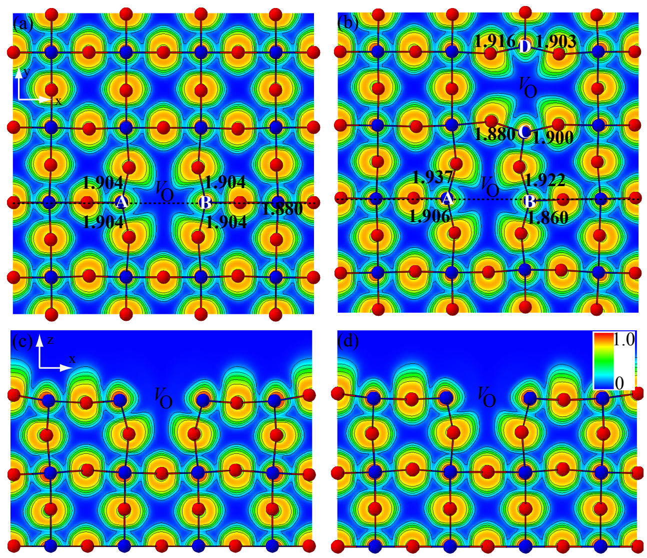

FIG. 3. Top views of the relaxed atomic positions and electron localization function (ELF) of TiO_2-terminated STO (001) surfaces with (a) a single oxygen vacancy and (b) the 0-4 divacancy. (c) and (d) are the side views when cutting a slice along the dashed line in (a) or (b). Titanium and oxygen atoms are represented by blue and red spheres, respectively. Ti-O bond lengths are numerically labeled in units of Å. The vacancies are located at the V_O positions. The color bar of ELF is shown in the inset of (d).

vacancies in bulk STO.[38]

Figure 1(b) shows the calculated $E_{\rm int}$ for different divacancies at the STO (001) surfaces. At the TiO_2-terminated surface, the 0-4 oxygen divacancy exhibits reduced repulsion compared to other divacancy arrangements, implying that divacancies at the surface tend to order along specific crystallographic directions, in this case along the <1,3> set of directions on the surface. We note that this vacancy ordering pattern is consistent with cluster expansion predictions.[39] We tested the sensitivity of these results to a different pair of U and J parameters, e.g., $U = 3.2$ eV and $J = 0.90$ eV, which were used in Ref.[38], and found slightly different interaction energies for the 0-3 and 0-4 divacancies (different by 0.025 and 0.042 eV, respectively), indicating that these interactions are not highly sensitive to the choice of U.

The interaction energies at the SrO-terminated surface are significantly less repulsive than for the TiO_2 termination. This is due to the fact that the SrO layer is more ionic than the TiO_2 layer leading to a significant amount of screening between the neutral oxygen vacancies, thereby reducing the repulsion between them. The interaction energy nevertheless has a non-monotonic function of distance suggesting that its subtle variations are possibly due to other electronic and structural couplings to the underlying STO lattice. The 0-5 divacancy at the SrO-terminated surface is the most stable configuration, suggesting a strikingly different vacancy ordering pattern, where three chains of oxygen atoms lie between the 0 and 5 vacancy sites as shown in Fig. 1(a). Due to the low interaction energies of the 0-4 and 0-5 divacancies at the TiO_2 and SrO-terminated surfaces, respectively, we henceforth narrow our discussion to these two specific divacancies.

The inclusion of a single vacancy or divacancy has two key effects on the STO (001) surfaces. First, the vacancies cause structural distortions of surrounding Ti-centered octahedra. The distortions can be seen from Fig. 3, which shows the optimized TiO_2 layers consisting of a single vacancy and the 0-4 divacancy. At the TiO_2-terminated surface (Fig. 3(a)), a single oxygen vacancy leads to a notable readjustment of the atomic positions of its neighboring Ti atoms; Ti_A and Ti_B. Here, the atomic rearrangement is symmetric. For example, the annotated Ti-O bond lengths in Fig. 3(a) are identical (1.904 Å). However, the appearance of a divacancy breaks the symmetry and results in different Ti-O bond lengths, as denoted in Fig. 3(b). This is most evident for the 0-4 oxygen divacancy which significantly reduces the otherwise local cubic symmetry, strongly coupling to octahedral tilts. The interaction energy is strongly reduced because of the additional relaxation under this reduced symmetry. In addition, there is a slightly compressive tetragonal distortion of 1%. This exemplifies the importance of the interactions between the two single vacancies and how their ordering along different directions couple to structural distortions in perovskites.

The structural distortions due to the vacancies at the SrO-terminated are less significant. Figures 4(c) and 4(d) show the cross-sectional views along the dashed line drawn in (a) and (b) for the relaxed atomic geometries in the presence of a single and the lowest energy 0-5 divacancy arrangement, respectively. The Ti-O bond lengths around the vacancy are only slightly smaller than the theoretical bulk STO value of 1.98 Å. An additional vacancy (i.e. a divacancy) has negligible effects on the structural distortions. This can be inferred from the minimal changes in bond lengths, depicted in Fig. 4(d). Unlike the TiO_2-terminated surface where the vacancies are strongly coupled via octahedral distortions because they are comprised of sites of equatorial oxygen atoms occupying the octahedra, the vacancies in the SrO-termination are in the apical sites of the octahedra and therefore are not strongly coupled to in-plane octahedral distortions. The strong interactions between equatorial oxygen vacancies was also recently seen in bulk $CaMnO_3$.[21] Also, the increased ionicity of the SrO-layer, as seen in the ELF (Figure 4(b)), leads to a stronger screening of oxygen vacancies, thereby significantly reducing its repulsive interaction energy for all possible configurations as compared to divacancies in a TiO_2 layer. This agrees with the much lower divacancy interaction energies that are seen at the SrO-terminated STO (001) surface. Since the vacancies on the SrO-terminated surface are created by removing underbonded oxygen atoms that essentially bind to the underlying Ti atom via hybridization with its d_{z^2} orbitals, the removal of an oxygen ion leads to

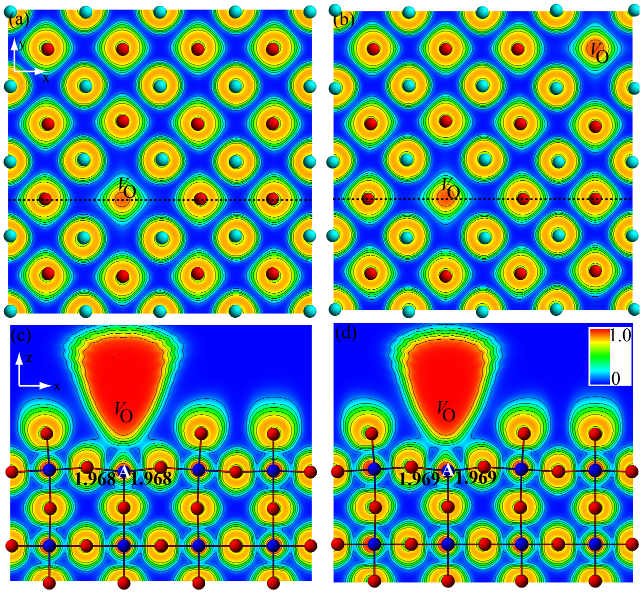

FIG. 4. Top views of the relaxed atomic positions and electron localization function (ELF) of SrO-terminated STO (001) surfaces with (a) a single oxygen vacancy and (b) the 0-5 divacancy. (c) and (d) are the side views when cutting a slice along the dashed line in (a) or (b). Strontium, titanium, and oxygen atoms are represented by cyan, blue, and red spheres, respectively. Ti-O bond lengths are numerically labeled in units of Å. The vacancies are located at the V_O positions. The color bar of ELF is shown in the inset of (d).

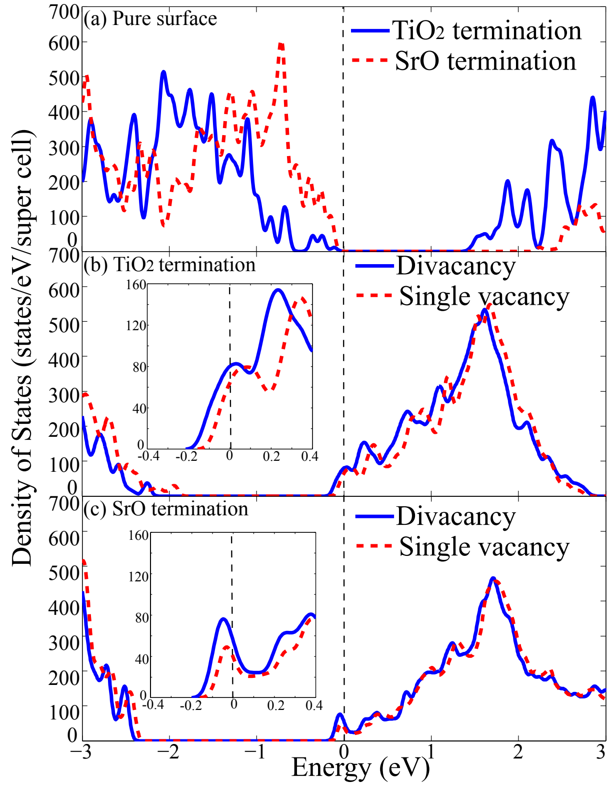

FIG. 5. DOS of (a) pure STO (001) surfaces with TiO_2 (solid blue line) and SrO (red dashed line) terminations. (b) and (c) are DOS of TiO_2 and SrO-terminated STO (001) surfaces with vacancies, respectively. Inset figures show DOS around the Fermi level.

a strong electron localization, much more than is seen on the TiO_2 layer. This is a key result, which demonstrates how the localization of electrons on the STO surface strongly differ between the two surface terminations.

It has been previously shown that single oxygen vacancies (albeit at high vacancy densities) create metallic states on STO (001) surfaces.[11] Here, we investigate the role of surface divacancies in the emergence of metallic surface states and contrast these with our results for single oxygen vacancies. Figures 5(b) and 5(c) show the density of states (DOS) of the two STO (001) surface terminations with a single oxygen vacancy and the 0-4 (TiO_2 surface) and 0-5 (SrO surface) divacancies. The DOS of pure STO surfaces with both the TiO_2 and SrO terminations are shown in Fig. 5(a) for the sake of comparison and as expected they remain insulating with computed band gaps of 1.36 and 2.14 eV, respectively. These two bandgaps are both smaller than our bulk STO GGA + U bandgap (2.21 eV).

Figures 5(b) and 5(c) confirm that STO (001) surfaces with a single vacancy and the 0-4 and 0-5 divacancies become metallic. For both surface terminations, the inset depicts the DOS around the Fermi level that contributes to the metallicity. Other types of divacancy ordering lead to similar metallicity as shown in Fig. 6. To assess whether the metallic states found at the STO (001) surface systems with single vacancies or divacancies

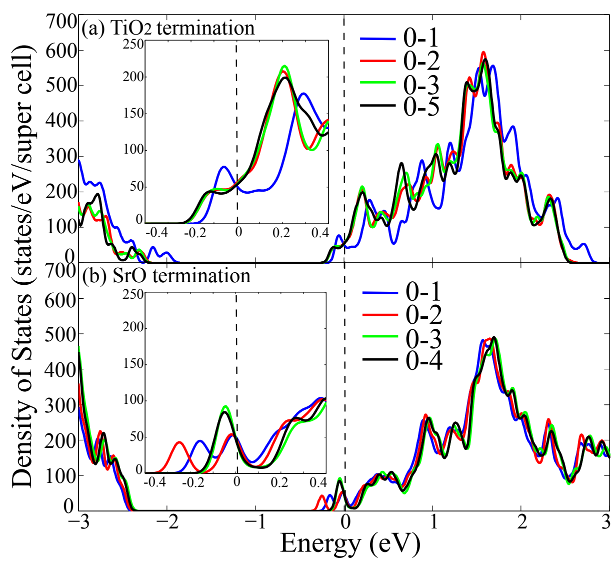

FIG. 6. DOS of (a) TiO_2 and (b) SrO-terminated STO (001) surfaces consisting of different divacancies with high interaction energies.

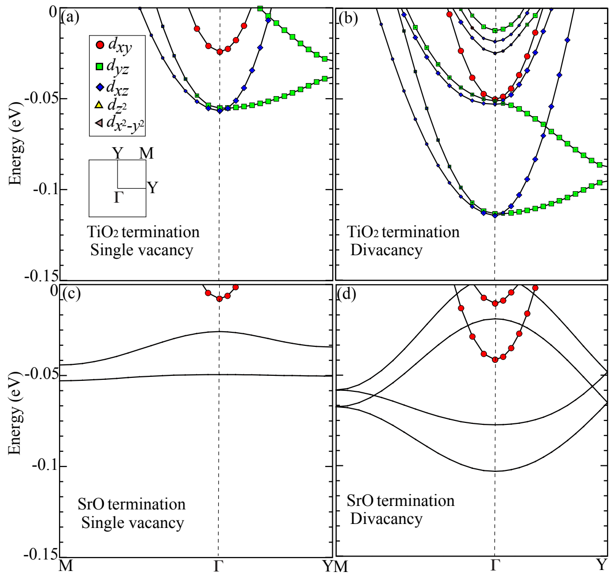

FIG. 7. GGA + U orbital projected valence band structures of TiO_2-terminated STO (001) surfaces with (a) a single oxygen vacancy and (b) the 0-4 divacancy. (c) and (d) are similar band structures for SrO-terminated STO (001) surfaces. The first Brillouin zone of the surface slabs as well as the corresponding high-symmetry K points are shown in the inset of (a). The continuous lines that form the bands are merely a guide to the eye and no disentanglement has been performed. Heavy bands in (c) and (d) mainly consist of d_{z^2} orbitals. However, the weights of these orbital contributions are too small to be illustrated on the same scale.

give rise to a 2DEG, we examine their band structures around the Fermi level (Fig.7). For the TiO_2-terminated surface with a single vacancy and divacancy, three and eight bands cross the Fermi level, respectively. On the other hand, for the SrO-terminated surface, only one and three bands cross the Fermi level. However, two common features are shared by all four band structures: (i) the parabolic band dispersions observed at the Γ point. Such dispersive bands are a typical indicator of the appearance of a 2DEG.[40] (ii) Lower symmetry in the presence of a divacancy leads to significant band splittings around the Γ point. The fat band analysis in Fig.7 indicates that the metallic carriers are mainly in the Ti-d orbitals. Due to the octahedral crystal field splitting, it is mainly the t_{2g} orbitals that participate in the metallicity, but because of the local symmetry reducing distortions there are additional subband splittings leading to their unequal electron filling. On the TiO_2-terminated surface, the d_{xz} and d_{yz} orbitals show increased contribution to the metallicity than the d_{xy} orbital. In the case of the SrO-termination, the metallicity comes mainly from the nearest TiO_2 layer and has predominantly a d_{xy} character. But due to localization of the electron, heavier bands are also seen in the gap.

To understand which atomic layers participate in the metallicity we plot the layer decomposed PDOS in Fig. 8 and Fig. 9, for the TiO_2 and SrO-terminated surfaces, respectively. At the TiO_2-terminated surface, the tetragonal splitting leads to increased occupation of the d_{xz} and d_{yz} orbitals compared to the d_{xy} orbital. The degree of this splitting decreases in layers below the defective layer. Looking at the total d-orbital DOS we find that the metallicity has much higher contributions from the TiO_2 layer just below the defective top surface. It is worth noting that the occupation of the d_{xz} and d_{yz} orbitals versus the d_{xy} is different than previously observed in STO/$LaAlO_3$ heterostructures or δ-doped STO. This is dependent on the degree of tetragonal splitting. In our case, the c/a $\sim$0.992 for the TiO_2-terminated surface and $\sim$0.975 for the SrO-terminated surface in the presence of divacancies. Tight-binding simulations, suggest that there is strong orbital ordering and as a result the d_{xy} orbitals are strongly localized and therefore in a two carrier model they represent the high density, low mobility carriers.[41] Conversely, the d_{xz} and d_{yz} orbitals have non-zero hopping parameters (but lower carrier densities) and are therefore low density, high mobility carriers. As such, the increase in the relative populations of the two may signal an enhancement in the overall mobility of these carriers. Such changes in orbital populations are thought to be the origin of the higher mobilities observed in fractionally δ-doped superlattices.[42]

Interestingly, for the SrO-termination, in addition to the flat defect band as seen in Fig. 7, which is predominantly of d_{z^2} character (Fig. 9), the 2DEG is mainly derived from the d_{xy} orbitals (which suggest that they would be strongly localized and perhaps have low mobilities due to orbital ordering). Interestingly, both TiO_2 layers below the surface significantly contribute to the 2DEGs, but their contribution is still much smaller than what is seen on a TiO_2-terminated surface. The common aspect in both terminations is that the metallicity is mainly coming from the TiO_2 layers with the layer closest to the defective surface contributing the most towards metallicity.

IV. CONCLUSIONS

In summary, we have systematically investigated the role of divacancies at $SrTiO_3$ (001) surfaces using the DFT+U method. We find that vacancy interaction energies are generally less repulsive on the SrO-terminated surface than on the TiO_2 terminated surface due to the increased ionicity of the SrO bond. On the TiO_2 surface, we observe strong directional ordering on the TiO_2 surface which is due to the coupling of vacancy sites to the local octahedral tilts. This results in a significant reduction in the repulsion for the 0-4 divacancy ordered along the crystallographic <1,3> direction. The low 0.05 eV and 0.38 eV interaction energies suggest that these short-ranged ordered vacancies should be visible by, e.g. electron microscopy at finite temperature. At higher vacancy concentrations, these types of divacancies could form e.g., long-ranged line defects that interact with each other to

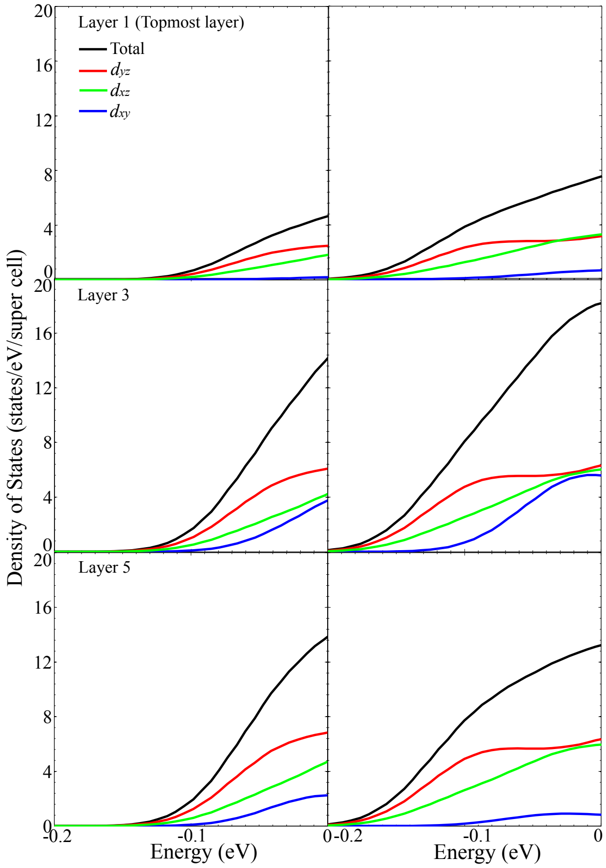

FIG. 8. Layer resolved PDOS for a single vacancy (left column) and the 0-4 divacancy (right column) on the TiO_2-terminated surface. Because only the TiO_2 layers contribute to metallicity, decomposition of the DOS is shown for the top three distinct TiO_2 layers for each case.

form clusters. The coupling between ordering direction and local octahedral distortions suggests that this effect may be a general phenomena in ABO_3 compounds and needs thorough investigation. Both terminations exhibit some metallic character in the presence of single vacancies and divacancies, which is confined to the TiO_2 layers. In all cases, the resultant two-dimensional electron gas lies mainly in the t_{2g} orbitals of the Ti-atoms with the TiO_2 layer closest to the defective layer having the largest occupations. In the case of the SrO-termination, oxygen vacancies lead to a strongly localized surface state. This suggests that while TiO_2-terminated layers can be adequately doped to increase metallicity and 2DEG character, SrO-terminated surfaces are in general good for thermoelectric applications due to the heavy bands.[31] While the current study focus on oxygen vacancies and divacancies, the rich physics here suggests the necessity of a comprehensive study of the different types of atomic defects and interactions between them in ABO_3 bulk systems and heterostructures using, e.g. a high throughput methodology.

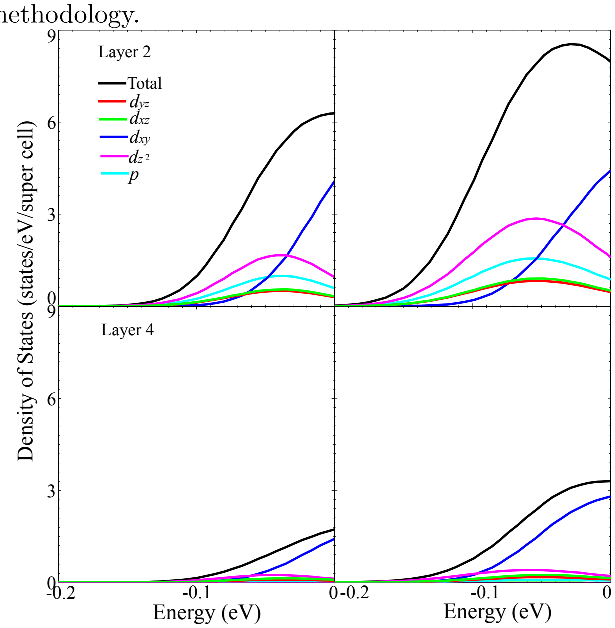

FIG. 9. Layer resolved PDOS for a single vacancy (left column) and the 0-5 divacancy (right column) on the SrO-terminated surface. Because only the TiO_2 layers contribute to metallicity, decomposition of the DOS is shown for the top two distinct TiO_2 layers in each case.

ACKNOWLEDGMENTS

Research sponsored by the Laboratory Directed Research and Development Program of Oak Ridge National Laboratory, managed by UT-Battelle, LLC, for the U. S. Department of Energy, and (HX) The University of Tennessee (UT) Science Alliance Joint Directed Research and Development Program (JDRD) and UT/ORNL Joint Institute of Advanced Materials (JIAM). This research used resources of the National Energy Research Scientific Computing Center, which is supported by the Office of Science of the U.S. Department of Energy under Contract No. DE-AC02-05CH11231.

* zhuanghl@ornl.gov
† ganeshp@ornl.gov

1 A. Ohtomo and H. Hwang, Nature **427**, 423 (2004).
2 P. Perna, D. Maccariello, M. Radovic, U. Scotti di Uccio, I. Pallecchi, M. Codda, D. Marr, C. Cantoni, J. Gazquez, M. Varela, S. J. Pennycook, and F. M. Granozio, Applied Physics Letters **97**, 152111 (2010).
3 J. Son, J. M. LeBeau, S. J. Allen, and S. Stemmer, Applied Physics Letters **97**, 202109 (2010).
4 L. Yu and A. Zunger, (2014), http://arxiv.org/abs/1402.0895.

[5] M. Gu, J. Wang, X. S. Wu, and G. P. Zhang, The Journal of Physical Chemistry C **116**, 24993 (2012).
[6] A. Kalabukhov, R. Gunnarsson, J. Börjesson, E. Olsson, T. Claeson, and D. Winkler, Phys. Rev. B **75**, 121404 (2007).
[7] A. F. Santander-Syro, O. Copie, T. Kondo, F. Fortuna, S. Pailhes, R. Weht, X. G. Qiu, F. Bertran, A. Nicolaou, A. Taleb-Ibrahimi, P. Le Fevre, G. Herranz, M. Bibes, N. Reyren, Y. Apertet, P. Lecoeur, A. Barthelemy, and M. J. Rozenberg, Nature **469**, 189 (2011).
[8] W. Meevasana, P. D. C. King, R. H. He, S.-K. Mo, M. Hashimoto, A. Tamai, P. Songsiriritthigul, F. Baumberger, and Z.-X. Shen, Nature Mater. **10**, 114 (2011).
[9] M. Kim, C. Bell, Y. Kozuka, M. Kurita, Y. Hikita, and H. Y. Hwang, Phys. Rev. Lett. **107**, 106801 (2011).
[10] Y. Li, S. N. Phattalung, S. Limpijumnong, J. Kim, and J. Yu, Phys. Rev. B **84**, 245307 (2011).
[11] J. Shen, H. Lee, R. Valentí, and H. O. Jeschke, Phys. Rev. B **86**, 195119 (2012).
[12] A. R. Silva and G. M. Dalpian, Journal of Applied Physics **115**, 033710 (2014).
[13] F. El-Mellouhi, E. N. Brothers, M. J. Lucero, and G. E. Scuseria, Journal of Physics: Condensed Matter **25**, 135501 (2013).
[14] C. Mitra, C. Lin, J. Robertson, and A. A. Demkov, Phys. Rev. B **86**, 155105 (2012).
[15] L. Suescun, O. Chmaissem, J. Mais, B. Dabrowski, and J. D. Jorgensen, Journal of Solid State Chemistry **180**, 1698 (2007).
[16] L. Suescun, B. Dabrowski, J. Mais, S. Remsen, J. W. Richardson, E. R. Maxey, and J. D. Jorgensen, Chemistry of Materials **20**, 1636 (2008).
[17] Y.-M. Kim, J. He, M. D. Biegalski, H. Ambaye, V. Lauter, H. M. Christen, S. T. Pantelides, S. J. Pennycook, S. V. Kalinin, and A. Y. Borisevich, Nature materials **11**, 888 (2012).
[18] R. Mishra, Y.-M. Kim, J. Salafranca, S. K. Kim, S. H. Chang, A. Bhattacharya, D. D. Fong, S. J. Pennycook, S. T. Pantelides, and A. Y. Borisevich, Nano Letters **14**, 2694 (2014).
[19] N. Biškup, J. Salafranca, V. Mehta, M. P. Oxley, Y. Suzuki, S. J. Pennycook, S. T. Pantelides, and M. Varela, Phys. Rev. Lett. **112**, 087202 (2014).
[20] Y. Du, X. Wang, D. Chen, Y. Yu, W. Hao, Z. Cheng, and S. X. Dou, Phys. Chem. Chem. Phys. **15**, 20010 (2013).
[21] U. Aschauer, R. Pfenninger, S. M. Selbach, T. Grande, and N. A. Spaldin, Phys. Rev. B **88**, 054111 (2013).
[22] G. Kresse and J. Furthmüller, Phys. Rev. B **54**, 11169 (1996).
[23] P. E. Blöchl, Phys. Rev. B **50**, 17953 (1994).
[24] G. Kresse and D. Joubert, Phys. Rev. B **59**, 1758 (1999).
[25] S. L. Dudarev, G. A. Botton, S. Y. Savrasov, C. J. Humphreys, and A. P. Sutton, Phys. Rev. B **57**, 1505 (1998).
[26] Z. Wang, M. Okude, M. Saito, S. Tsukimoto, A. Ohtomo, M. Tsukada, M. Kawasaki, and Y. Ikuhara, Nature Comm. **1**, 106 (2010).
[27] H. J. Monkhorst and J. D. Pack, Phys. Rev. B **13**, 5188 (1976).
[28] N. P. Guisinger, T. S. Santos, J. R. Guest, T.-Y. Chien, A. Bhattacharya, J. W. Freeland, and M. Bode, ACS Nano **3**, 4132 (2009).
[29] A. M. Ritzmann, A. B. Munoz-Garcia, M. Pavone, J. A. Keith, and E. A. Carter, Chemistry of Materials **25**, 3011 (2013).
[30] H. Cheng and A. Selloni, Phys. Rev. B **79**, 092101 (2009).
[31] Z. Wang, Z. Zhong, X. Hao, S. Gerhold, B. Stöger, M. Schmid, J. Sanchez-Barriga, A. Varykhalov, C. Franchini, K. Held, and U. Diebold, Proceedings of the National Academy of Sciences **111**, 3933 (2014).
[32] H. Xu, D. Lee, J. He, S. B. Sinnott, V. Gopalan, V. Dierolf, and S. R. Phillpot, Phys. Rev. B **78**, 174103 (2008).
[33] P. Linstrom and W. G. Mallard, eds., NIST Chemistry WebBook, NIST Standard Reference Database, Vol. 69 (National Institute of Standards and Technology) http://webbook.nist.gov, retrieved 26 May 2014.
[34] D. Gryaznov, E. Blokhin, A. Sorokine, E. A. Kotomin, R. A. Evarestov, A. Bussmann-Holder, and J. Maier, The Journal of Physical Chemistry C **117**, 13776 (2013).
[35] J. Carrasco, F. Illas, N. Lopez, E. A. Kotomin, Y. F. Zhukovskii, R. A. Evarestov, Y. A. Mastrikov, S. Piskunov, and J. Maier, Phys. Rev. B **73**, 064106 (2006).
[36] E. Ertekin, V. Srinivasan, J. Ravichandran, P. B. Rossen, W. Siemons, A. Majumdar, R. Ramesh, and J. C. Grossman, Physical Review B **85**, 195460 (2012).
[37] Y. Zhang and W. Yang, Physical Review Letters **80**, 890 (1998).
[38] D. D. Cuong, B. Lee, K. M. Choi, H.-S. Ahn, S. Han, and J. Lee, Phys. Rev. Lett. **98**, 115503 (2007).
[39] P. Ganesh, H. Zhuang, P. R. C. Kent, V. R. Cooper, and H. Xu, Unpublished.
[40] N. Sivadas, H. Dixit, V. R. Cooper, and D. Xiao, Phys. Rev. B **89**, 075303 (2014).
[41] S. Okamoto, A. J. Millis, and N. A. Spaldin, Phys. Rev. Lett. **97**, 056802 (2006).
[42] W. S. Choi, S. Lee, V. R. Cooper, and H. N. Lee, Nano Letters **12**, 4590 (2012).